NeuroImage 46 (2009) 345–352

Contents lists available at ScienceDirect

NeuroImage

journal homepage: www.elsevier.com/locate/ynimg

On the origin of the MR image phase contrast: An in vivo MR microscopy study of the rat brain at 14.1 T

José P. Marques [a,b,*], Rajika Maddage [a], Vladimir Mlynarik [a], Rolf Gruetter [a,b,c]

[a] Laboratory for Functional and Metabolic Imaging, Ecole Polytechnique Federale de Lausanne, Switzerland
[b] Department of Radiology, University of Lausanne, Lausanne, Switzerland
[c] Department of Radiology, University of Geneva, Geneva, Switzerland

ARTICLE INFO

Article history:
Received 11 September 2008
Revised 18 December 2008
Accepted 16 February 2009
Available online 27 February 2009

Keywords:
Phase imaging
In vivo rat brain
High field MRI
Contrast mechanisms

ABSTRACT

Recent studies at high magnetic fields using the phase of gradient-echo MR images have shown the ability to unveil cortical substructure in the human brain. To investigate the contrast mechanisms in phase imaging, this study extends, for the first time, phase imaging to the rodent brain. Using a 14.1 T horizontal bore animal MRI scanner for in vivo micro-imaging, images with an in-plane resolution of 33 μm were acquired.

Phase images revealed, often more clearly than the corresponding magnitude images, hippocampal fields, cortical layers (e.g. layer 4), cerebellar layers (molecular and granule cell layers) and small white matter structures present in the striatum and septal nucleus. The contrast of the phase images depended in part on the orientation of anatomical structures relative to the magnetic field, consistent with bulk susceptibility variations between tissues. This was found not only for vessels, but also for white matter structures, such as the anterior commissure, and cortical layers in the cerebellum.

Such susceptibility changes could result from variable blood volume. However, when the deoxyhemoglobin content was reduced by increasing cerebral blood flow (CBF) with a carbogen breathing challenge, contrast between white and gray matter and cortical layers was not affected, suggesting that tissue cerebral blood volume (and therefore deoxyhemoglobin) is not a major source of the tissue phase contrast.

We conclude that phase variations in gradient-echo images are likely due to susceptibility shifts of non-vascular origin.

Introduction

While most contrast mechanisms in MRI exploit differences in relaxation (T_1-, T_2- or T_2*-weighting), or spins mobility (perfusion and diffusion imaging), contrast in susceptibility-weighted imaging is partially based on variations in signal phase (Haacke et al., 2004). In human brain this has been used to detect veins and iron rich regions (Haacke et al., 2004) and contrast between WM and cortical GM (Abduljalil et al., 2003; Duyn et al., 2007). As the variations in the signal phase scale with the static magnetic field strength, the increasingly strong magnets available promise the ability to detect additional anatomical information using solely this information. While the precise mechanism giving rise to tissue variations in phase is at present unknown, tissue susceptibility variations (Duyn et al., 2007) or the content of macromolecules affecting the water chemical shift (Zhong et al., 2008) have been suggested to contribute to such phase variation. Tissue susceptibility changes may be due to different tissues deoxyhemoglobin content (via regional differences in CBV), iron or lipid content (Duyn et al., 2007), or, in some pathological conditions, high calcium concentration (Hammond et al., 2008).

Animal models can be used to shed light on the aforementioned putative contrast mechanisms, by either manipulating the physiological conditions, or by studying suitable disease models. Second, it is easier to perform postmortem studies whether by MR imaging or histochemistry. Finally, in animal MRI a much higher spatial resolution can be achieved, reducing partial volume effects.

Most very high resolution rodent studies (Badea et al., 2007; Benveniste et al., 2000; Johnson et al., 2007) have been performed on ex-vivo samples, allowing for long acquisition times without physiological noise or motion. Some of the advantages of imaging ex-vivo were demonstrated in a recent study (Jack et al., 2004, 2005), where in Alzheimer mouse models amyloid plaques were identified using spin echo MRI. Interestingly, the smallest observable plaques in vivo had an apparent dimension of 35 μm whilst *ex vivo* their dimensions were 20 μm. One limitation of postmortem studies is that after tissue fixation the MR relaxation parameters may be altered, providing a potentially different contrast from that obtained in vivo (Benveniste and Blackband, 2006).

At present, few reports have used phase imaging in animal models. In fact, to our knowledge, only one study has been published

* Corresponding author. Laboratory for Functional and Metabolic Imaging, Ecole Polytechnique Federale de Lausanne, Switzerland.
E-mail address: jose.marques@epfl.ch (J.P. Marques).

1053-8119/$ – see front matter © 2009 Elsevier Inc. All rights reserved.
doi:10.1016/j.neuroimage.2009.02.023

using the related, but distinct, method of susceptibility-weighted imaging (SWI) in rodents (Park et al., 2008). The increasing static magnetic field strengths available for animal studies (from 7 to 21 T) offer a signal gain associated with high magnetic fields, together with an increased frequency shift distribution. These can be exploited in phase imaging to increase spatial resolution and reduce scanning time, therefore reducing physiological variability and likelihood of animal movements. The aim of the present study was to take advantage of a 14.1 T horizontal bore system to assess the observable contrast in the in-vivo rat brain using both magnitude and phase gradient-echo (GRE) images with an in-plane resolution of ~30 μm.

Materials and methods

All studies were performed on a 14.1 T/26 cm scanner (Varian/Magnex Scientific) using a home built quadrature surface coil as RF transceiver with two geometrically decoupled 14 mm loops resonating at 600 MHz. Such a setup provides high SNR, due to the high B_0 and maximum coil sensitivity achieved by optimizing the filling factor for the rat brain. The main drawbacks of surface coils are the inhomogeneous transmit and receive B_1 field. The flip angle was set to allow deep brain coverage while avoiding undesirable inversions in the regions closest to the coil. This yielded sufficient SNR in deeper brain areas, despite the low coil sensitivity in such regions. In regions closer to the surface, the high coil sensitivity compensates the high flip angle. This approach gives a flatter magnitude image profile than might otherwise be expected for surface coils. In phase imaging, this is not as critical, as only the local SNR varies with the local signal amplitude. Another advantage of the use of surface coils is the possibility of using small field of views as the limited sensitivity away from the coil reduces wrap-around artifacts in the phase encoding direction.

The TR was set to match the respiration rate, which was controlled by a ventilator, significantly reducing respiration induced artifacts. TE was chosen to approximately match the gray matter T_2* and hence optimize phase contrast (Duyn et al., 2007; Gruetter, 1993). From an 18 Hz water spectra linewidth measured in well-shimmed small voxel containing white matter, gray mater and the hippocampus, T_2* was estimated to be 16 ms.

To minimize through-slice dephasing and image distortions, magnetic field homogeneity was adjusted using FASTMAP (Gruetter, 1993), in a large volume located in the hippocampus and striatum (when imaging the brain) or in the cerebellum (when imaging the cerebellum). Gradient-echo images of the rat brain were acquired with a nominal in-plane resolution of 33 μm, i.e., FOV = 17 × 12.7 mm (matrix size 512 × 382), slice thickness of 0.4 mm, TR/TE = 1100/16 ms with an acquisition time of 16 ms. The acquisition bandwidth was chosen in order to maximize signal without introducing effective resolution reduction due to T_2* decay during the readout. Each image was acquired in 6.3 min and nine repetitions were added to obtain the final images.

Five adult rats (Sprague–Dawley) were scanned under 2% isoflurane anesthesia. The animals were stereotaxically fixed with ear bars in a home-made holder. Throughout the experiments, animals were maintained under normal physiological conditions (rectal temperature ~38 °C, blood gas in pH ~7.4 and pCO_2 ~39 mm Hg, measured using a nearby AVL analyzer, Roche Diagnostics), while breathing 100% O_2. In four of these rats, to determine the influence of tissue deoxyhemoglobin content on the tissue phase images contrast, the arterial pCO_2 was increased on average to ~65 mmHg by increasing the inspired CO_2 fraction up to 5% (rectal temperature ~38 °C, blood gas in pH ~7.1). Increasing arterial pCO_2 is known to increase cerebral blood flow (Shockley and LaManna, 1988) without increasing oxygen metabolism ($CMRO_2$).

To determine the orientation dependence of the phase variation, a mouse brain was fixed by washing out the blood through perfusion of a physiological saline solution while under 2% isoflurane anesthesia. The fixed brain was scanned using the following parameters: TR/TE = 300/11 ms, FOV = 9 × 18 mm (in-plane resolution 35 μm), slice thickness of 0.3 mm, 10 averages. Images were obtained with the brain rotated 0, 22.5, 45, 67.5 and 90° in respect to the main magnetic field. The slice direction accompanied the mouse brain rotation, ensuring that comparable images would be obtained for all directions.

To remove the effect of large-scale phase shifts across the phase images, ascribed to large-scale B_0 inhomogeneities, a 2D Gaussian high-pass filter with a kernel size of 127 voxels and a width of 10 voxels was applied to all images to remove low-frequency phase variations (Noll et al., 1991). The magnitude data of the different measurements was simply added. The phase images from each measurement were calculated after the complex high-pass filter had been applied, and were only then averaged together. This procedure was performed to avoid SNR losses due to global phase drifts. No motion correction was applied before averaging.

Results

Axial images acquired with the surface coil show good coverage of almost the whole brain (Fig. 1a). The corresponding phase image (Fig. 1b) already allows detection of some of the tissue phase contrast despite regional B_0 shifts due to residual macroscopic B_0 variations. All phase images shown hereafter have been high-pass filtered and masked, as shown Fig. 1c, removing most of the phase variations due to macroscopic susceptibility effects.

High spatial resolution with negligible motion or respiration artifacts was routinely achieved, as illustrated by the detection of structures with widths of ~1 pixel such as some of the venules and capillaries visible in the magnitude and phase images shown in Fig. 2.

In phase images intersecting vessels perpendicular to B_0 (see Fig. 2b), field patterns extending beyond the vessel boundaries were observed. These non-local, extra-vascular, effects are similar to those generated by "infinite cylinders" with a homogenous susceptibility distribution, oriented perpendicular to the main magnetic field. These non-local effects can affect the apparent contrast of phase images in various ways

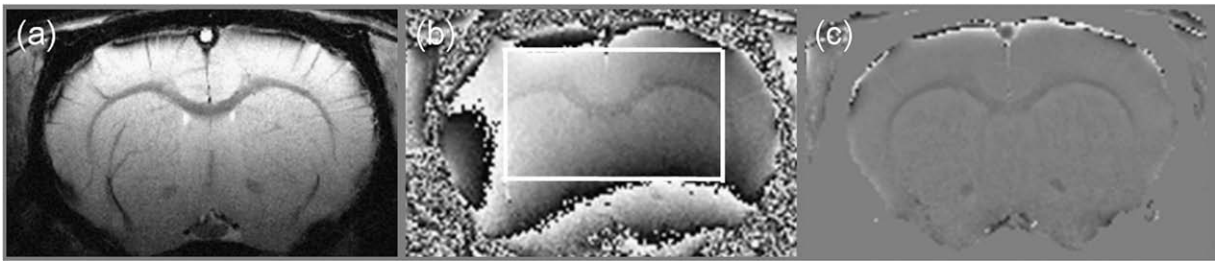

Fig. 1. Different reconstructions of a representative axial slice of the whole brain GRE acquisitions are shown: (a) magnitude, (b) phase and (c) phase image after filtering and masking. The white square represents the area where the shimming was performed.

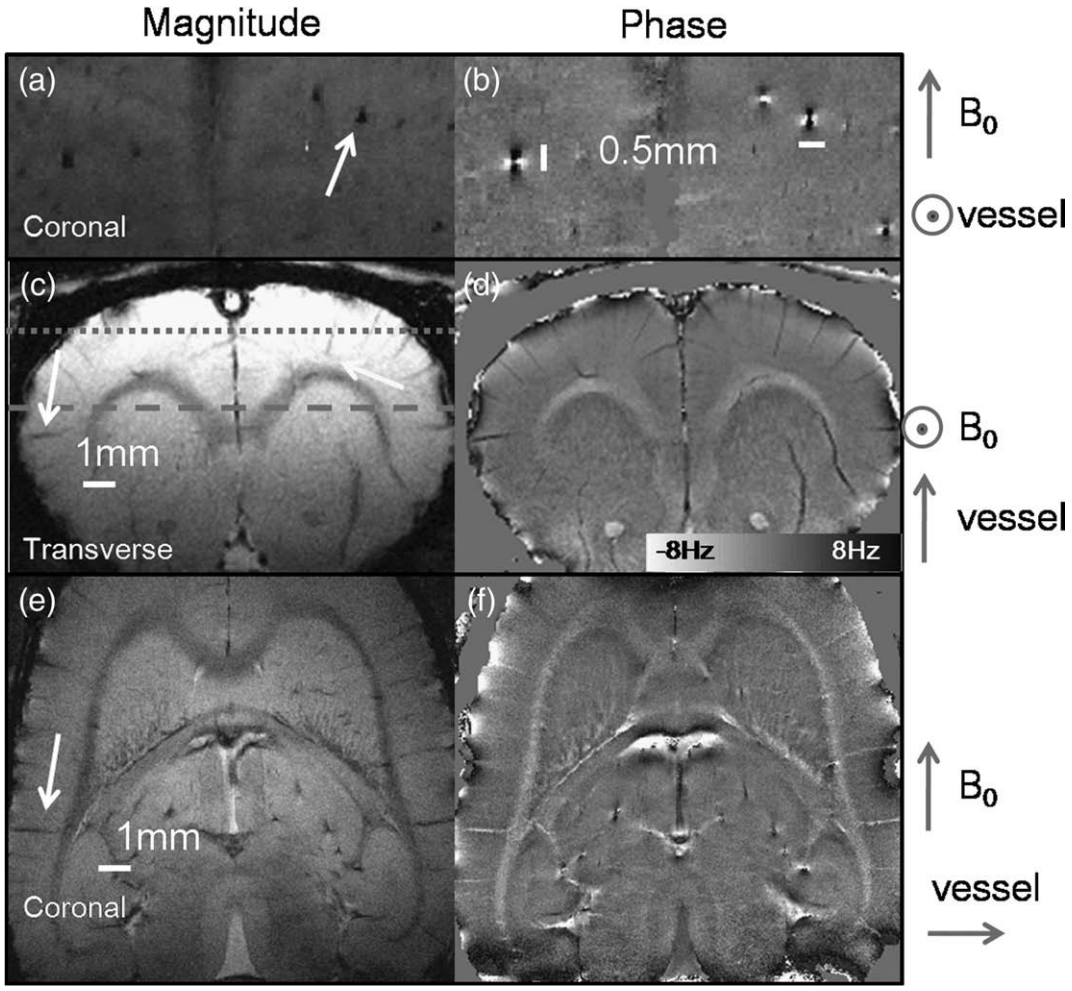

Fig. 2. Magnitude (a, c, e) and phase images (b, d, f) of a rat brain are shown on the left and right respectively. The coronal slices (a, b) and (e, f) are located at the region showed with the dotted and dashed lines respectively in the transverse slice (c). White arrows point different vessels of interest that are perpendicular to the magnetic field. On the right, the direction of the main magnetic field and vessels of interest are shown.

as shown in Figs. 2d and f. In the magnitude images (Figs. 2c and e), the vein-tissue contrast obtained was, as expected, independent of the slice orientation. However, in the phase images, vein-tissue contrast changed between coronal (Fig. 2d) and axial (Fig. 2f) slice orientations, even though all those vessels (pointed out by white arrows in Fig. 2) were perpendicular to the magnetic field and therefore feature the same dipole field distribution. When these vessels are in-plane they generate very different contrasts depending on whether the slice averaging was done along the magnetic field as in the axial image (Fig. 2d) or perpendicular to the magnetic field as in the coronal image (Fig. 2f). These effects can be demonstrated via simulations (Fig. 3) of the frequency map generated by an infinite cylinder of 40 μm. This map was computed using standard assumptions regarding blood oxygen concentration and deoxyhemoglobin susceptibility (Marques and Bowtell,

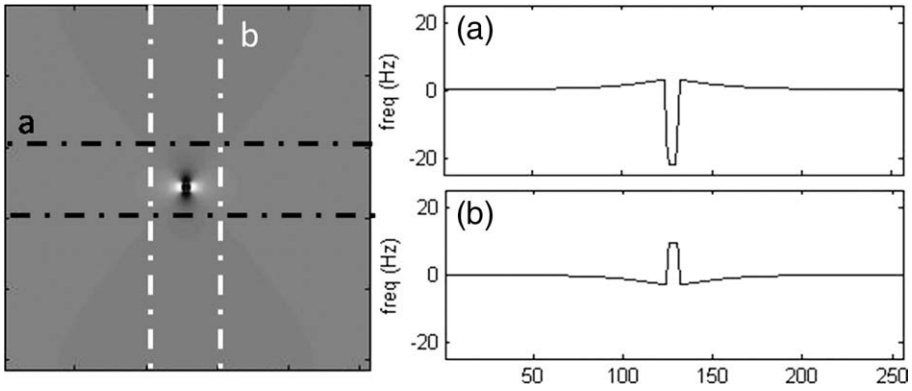

Fig. 3. Simulated frequency map of an infinite cylinder, of 40 μm radius, perpendicular to the magnetic field, of 14 T, with the susceptibility of 0.41 ppm (corresponding to a oxygen fraction of 0.55, an hematocrit content of 0.4 and assuming the magnetic susceptibility of deoxyhemoglogin to be 2.26 ppm in SI units). Dashed lines show the limits of an hypothetical axial (black) or coronal (white) slice of 500 μm. The resulting phase values from averaging across those slices are shown on plots (a) and (b).

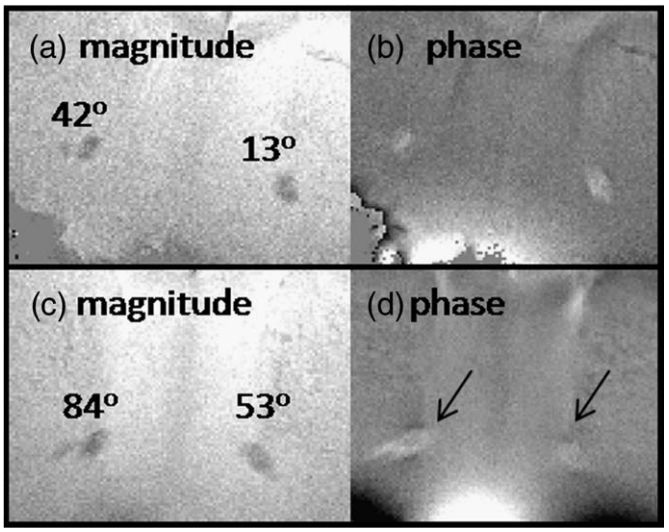

Fig. 4. Magnitude (a, c) and corresponding phase (b, d) images of a fixed mouse brain positioned in two different orientations in respect to the main magnetic field. The calculated angle between the AC and B_0 is indicated in the images magnitude images. The arrows in (d) point out to the magnetic susceptibility effect visible around the white matter tract.

2008). Averaging across a 500 μm thick slice along the B_0 direction (Fig. 3a) or a direction perpendicular to both B_0 and the vessel orientation (Fig. 3b), reproduced the vessel contrast visible in Fig. 2d and f respectively. This slice orientation-dependent contrast was thus ascribed to the averaging across a slice that is thicker than the structure of interest.

Clearly, the aforementioned dipole shape surrounding blood vessels orthogonal to the main magnetic field is due to susceptibility differences between blood in the vessels and the surrounding tissue. In contrast, the origin of the tissue phase contrast has remained less clear and other mechanisms, such as the macromolecular concentration, have been proposed (Zhong et al., 2008). While the B_0 intensity and echo time dependences of the phase images are expected to be the same for macromolecular and susceptibility mechanisms, only the latter is expected to be orientation dependent.

Therefore, to test whether the tissue contrast observed in white matter exhibits orientation dependence, we focused on the anterior commissure (AC), a cylinder-like white matter tract embedded in the striatum. A fixed mouse brain was imaged at different orientations with respect to the main magnetic field. Fig. 4 shows mouse brain images acquired with a 0 and 67.5° rotation relative to B_0. A dipole shape surrounding the AC was observed in the phase images only when the angle between the AC and B_0 approached 90° (Figs. 4a and c), similar to that of an infinite cylinder with a homogenous susceptibility, differing from that of the surrounding tissue.

To ascertain whether phase variations observed in the cortex were similarly orientation-dependent, the rat cerebellum was studied. Due to its topology, featuring both cortical surfaces parallel to B_0 as well as cortical surfaces perpendicular to B_0, the rat cerebellum allows the observation of putative orientation dependence without the need to perform brain rotations. Sagittal slices were chosen for visualization of

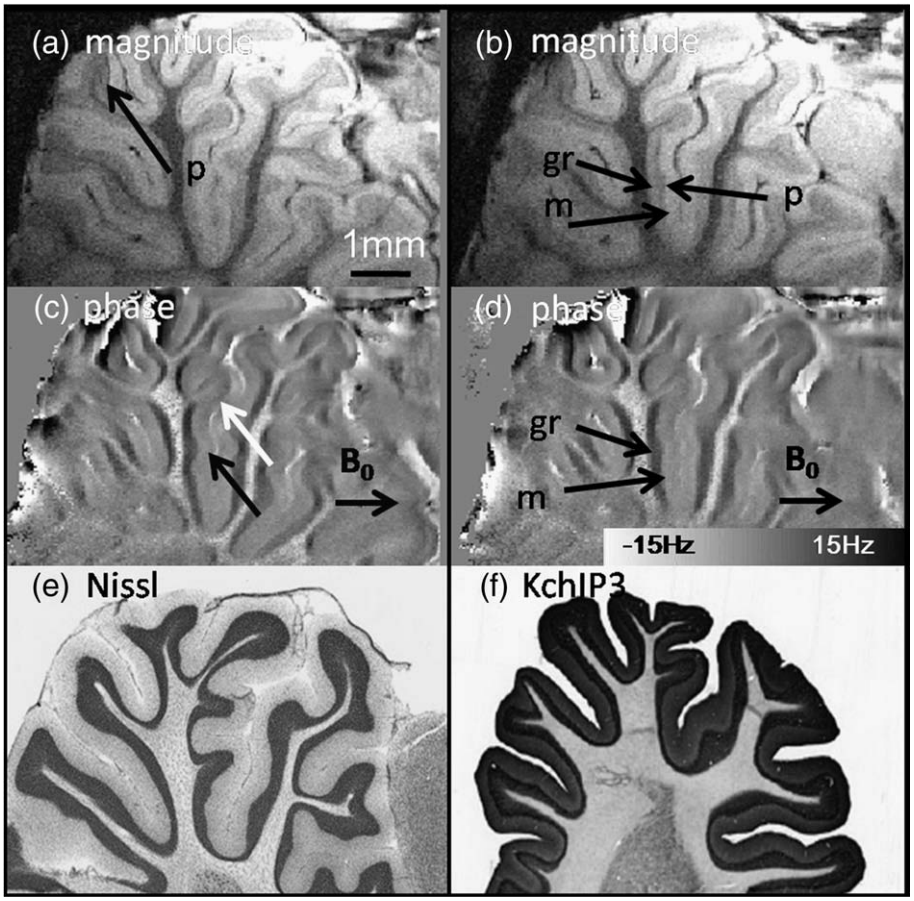

Fig. 5. Magnitude (a, b) and phase (c, d) sagittal images of the rat cerebellum at 14.1 T. Black arrows point: g — granule cell layer; m — molecular layer; p — Purkinje cell layer. The white arrow points a region where the dependence of the contrast between granule layer and molecular layer on the direction between B_0 and the cortical surface is very clear. Similar histochemistry slices obtained with Nissl staining (e) and KChIP3 (f) obtained from www.brainmaps.org (© The Regents of the University of California, Davis campus. Used with permission) and (Strassle et al., 2005) (Reprinted with permission of John Wiley & Sons, Inc.) respectively.

the medial section of the cerebellum where the structures vary little in the through-slice dimension, but vary significantly in the in-plane dimension, facilitating the observation of such putative orientation dependence in one single image. Magnitude images exhibited a strong contrast between the granule cell and molecular layers of the cerebellum (Figs. 5a and b), which had previously only been reported in-vivo following manganese infusion (Aoki et al., 2004), and the anatomy visible in these images clearly mimicked that observable in histochemistry slices obtained through Nissl staining (www.brainmaps.org) and KChIP3 (Strassle et al., 2005), shown in Figs. 5e and f. Only the Purkinje cell layer, located between the molecular and granule cell layers, with a thickness of approximately 15 μm (Strassle et al., 2005), was not as clearly observable, although the presence of a thin black structure was noted between the granule cell and molecular layers (Figs. 5a and b), both of which were clearly discernible (Figs. 5c and d). An unambiguous orientation dependence was observed for the granule cell layers: In Fig. 5 the main magnetic field B_0 points horizontally, and layers perpendicular to the magnetic field (black arrow in Fig. 5c) show a larger phase shift than layers that are closer to being parallel to B_0 (white arrow in Fig. 5c), suggesting that magnetic susceptibility is a substantial mechanism causing phase/frequency shifts also in the cortical layers detected in the cerebellum.

Throughout the brain, the high spatial resolution and unique contrast of axial phase images allowed the identification of smaller white matter structures that were less noticeable in the magnitude images. Striking examples were the fornix and mamillothalamic tract (arrows 4 and 5 in Fig. 6d) and the projection of white matter tracts from the external capsule into the internal capsule (arrow 3 in Fig. 6d). The mixed constitution of the caudate putamen – striatum and the septal nucleus (Fig. 6c, arrows 7 and 8), structures which are known to consist of a both gray and white matter was unmistakably observed. The anatomical detail observed in the phase images closely mimicked that from histochemistry in corresponding slices observed using KChIP1 staining (www.brainmaps.org) (Mikula et al., 2007). Differences between histochemistry section thickness (40 μm) and MR slice thickness (500 μm) are likely to explain some subtle differences, such as the white matter structures that in the histochemistry seem to be through-slice, having a more along-slice appearance in the phase images. In Figs. 6a and c, white matter tracts such as the corpus callosum (arrow 1, white matter tracts running in-plane) and the cingulum (arrow 6, white matter tracts running through-plane) have very different contrast both in the magnitude and phase images, which further points towards a direction-dependent susceptibility related dephasing and shift in the magnitude and phase images respectively.

In the phase images intersecting the hippocampus (Bregma slice −3.6 mm, Fig. 7b), not only veins and white matter structures were discernible but also gray matter layers and hippocampal fields such as the CA1 and dentate gyrus, which remained elusive in the magnitude images (Fig. 7a). The gray matter layers were consistently observed in all animals, but given their low contrast to the surrounding gray matter (~0.5 Hz), high SNR was needed for their clear visualization. SNR was sufficiently high in regions close to the receiver coil and the contrast thus became more elusive in regions more distal to the RF coil.

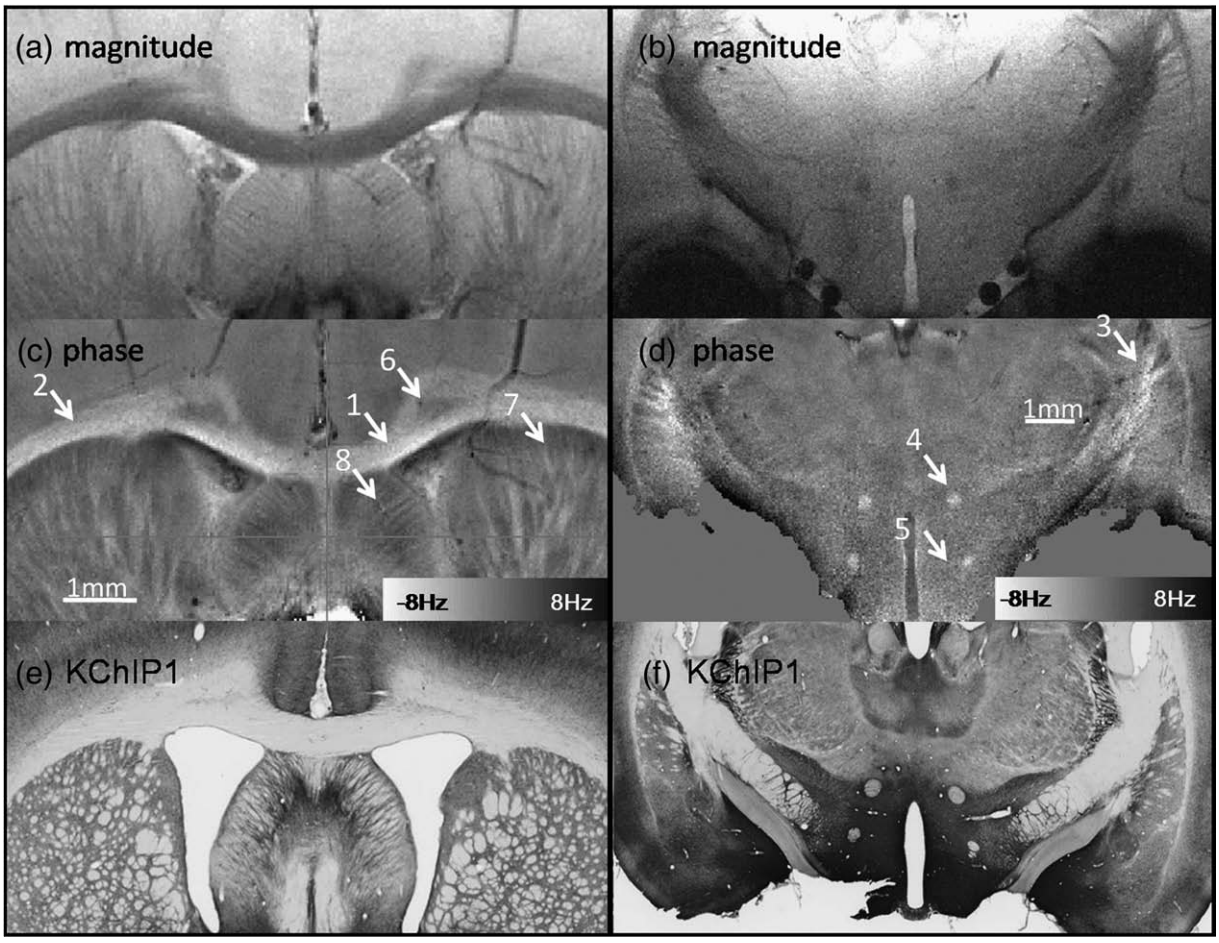

Fig. 6. Magnitude (a, b) and phase images (c, d) acquired at 14.1 T and similar brain histochemistry slices obtained with KChIP1 (e, f) (www.brainmaps.org © The Regents of the University of California, Davis campus. Used with permission.) axial cuts located at Bregma slice −0.4 mm (a, c, e) and −3.0 mm (b, d, f). Arrows point to some interesting white matter structures such as: 1 — corpus callosum, 2 — external capsule, 3 — internal capsule, 4 — fornix, 5 — mamillothalamic tract, 6 — cingulum; and some mixed white gray matter structures such as: 7 — caudate putamen – striatum, and 8 — septal nucleus.

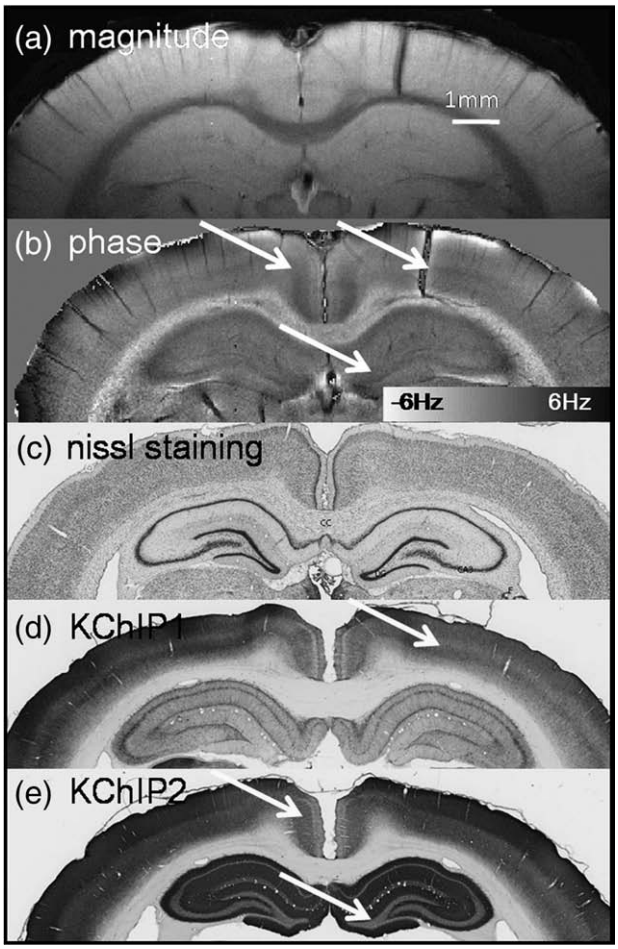

Fig. 7. Magnitude (a) and phase images (b) acquired at 14.1 T and similar brain histochemistry slices obtained with Nissl staining, KChIP1 and KChIP2 (c–e) (www.brainmaps.org © The Regents of the University of California, Davis campus. Used with permission.) axial cuts located at Bregma slice ~ − 3.6 mm. Arrows point different cortical layer regions visible in the phase imaging that are in good agreement with the histochemistry.

The anatomy observed was consistent with that observed in Nissl (cresyl violet) and voltage-gated Potassium channel interacting protein 1 and 2 (KChIP1 and KChIP2) stained brain slices (Figs. 7c, d and e respectively, www.brainmaps.org).

Deoxyhemoglobin (dHb) is widely accepted to be in the origin of the blood to tissue contrast as it is shown in Fig. 2. Since the brain has regional variations of cerebral blood volume (CBV), venous dHb may be at the origin of the contrast observed in phase imaging. To determine to what extent dHb contributes to the tissue contrast, such as that between white and gray matter and between cortical layers, the tissue dHb content was altered. Tissue dHb content was changed by increasing pCO_2, which has been shown to increase CBF markedly with marginal changes in oxygen consumption resulting in a net increase of oxygen in the venous effluent and thus a decrease in venous dHb. When comparing, phase images from animals breathing pure oxygen (Figs. 8a and b), with those from the same animals under carbogen breathing (Figs. 8c and d), it was clear that most of the tissue contrast was unaffected. The major changes observable were restricted to the veins. To illustrate that the tissue variation in the phase images was not affected by the reduced dHb content, the difference image was computed by complex division (Figs. 8e and f). Clearly, in the difference phase image (Fig. 8e) the contrast between white and gray matter, as well as that between, the cortical and hippocampal fields (Fig. 8f) disappeared to a large extent, while the veins remained visible, demonstrating that tissue dHB content was a minor contributor to the tissue contrast in the phase images. To quantify this visual impression, 63 projections perpendicular to the surface of gray matter, running to the centre of the hippocampus (Fig. 8d) were defined. Along the projections, 4 different regions were identified to accommodate for the different regional thickness of gray matter layers and white matter. While gray matter cortical layers and white matter were clearly distinguishable in these projections under at normal and elevated pCO_2 (blue and black lines in Fig. 8g), the difference projection was devoid of any variation (red line in Fig. 8g). It is of interest to note that even over extended time periods (over 1 h), difference phase images could be calculated with minimal motion artifacts despite a spatial resolution of 33 μm, which amounts to in vivo microscopy.

Discussion

The present study shows that high resolution gradient-echo imaging of the in vivo rat brain with long echo times and low bandwidth at fields as high as 14 T is possible yielding exceptional anatomical contrast. Phase contrast obtained at 14 T should not be specific to the magnetic field nor the echo time, as all proposed mechanisms are expected to scale linearly with B_0 and TE, but is

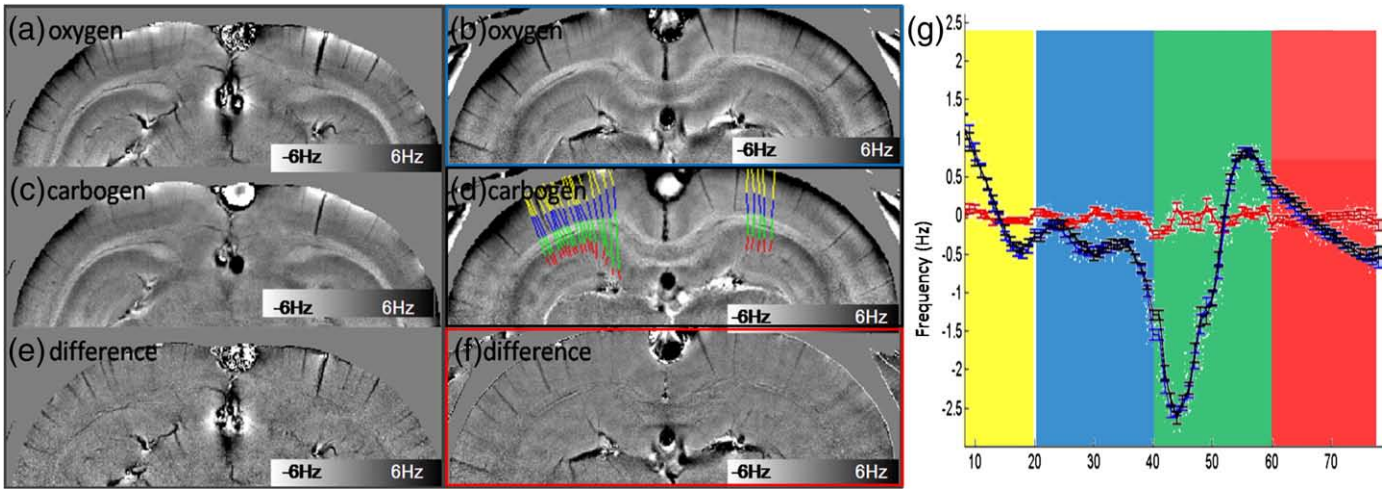

Fig. 8. Phase images from two different animals corresponding to oxygen (a, b), carbogen (c, d) breathing and the difference between both states (e, f). The phase difference image was computed via division of the complex images acquired during oxygen and during carbogen breathing. The lines in (d) represent the regions where the profiles in (g) were measured. In (g) the average profiles through GM, WM and hippocampus are shown in blue, black and red, corresponding to oxygen breathing, carbogen breathing and the difference. Each of the colored regions in the plot (g) corresponds to a stretch with the same colour (d).

expected to benefit at least linearly from increases in magnetic field (Duyn et al., 2007). To facilitate comparisons between the phase imaging contrasts obtained at different magnetic field strengths, frequency shifts could be converted to ppm as it is commonly done in spectroscopy.

In phase imaging the current standard of practice is to apply a high-pass filter which minimizes the influence of large-scale B_0 fields and eddy currents. A precise measurement of the tissue frequency shift would require the simultaneous measurement of an additional echo and calculation of the frequency map from the phase difference, similar to what is done in many field mapping approaches. However, this would result in reduced SNR, due to a shorter evolution time of the phase and higher bandwidth required (to sample the echoes in a shorter time). In this case, a high-pass filter would still be required to eliminate the aforementioned effects on large-scale phase shifts. Therefore, the relative frequency change between neighboring regions should be identical whether acquired from a field map or a phase image.

An orientation dependence of the phase variation in the images was noticed not only for the vessel phase shifts, but also in white matter and in the parenchyma of the cerebellum (Figs. 2, 4 and 5). Such orientation dependence suggests that tissue susceptibility induced magnetization is a major source of the phase variations observed. Therefore, the contrast seen in phase images is affected by an intrinsic non-locality and, at least in part, the result of a convolution of the susceptibility distribution with the magnetic dipole kernel (Marques and Bowtell, 2005). Significant difference in the phase contrast between the cingulum and corpus callosum points towards a subvoxel structure contribution to the phase variations. We therefore conclude that a significant mechanism yielding tissue phase variations is due to bulk susceptibility differences not only between gray and white matter but also within cerebellar gray matter structures.

Interestingly, although the white/gray matter contrast showed orientation dependence for the anterior commissure, it was not inverted on the fixed brain experiments when rotating the specimens by 90°, despite the angles between the AC and B_0 being varied from almost parallel (13°) to almost perpendicular (84°) to the main magnetic field. This may reflect the fact that the anterior commissure has a limited length and some curvature and thus is not an infinite cylinder or due to a partial contribution of macromolecular content to the phase, as proposed recently (Zhong et al., 2008).

Bulk susceptibility shifts can in principle be ascribed to variations in tissue deoxyhemoglobin content, we reduced the dHB content by increasing pCO_2, which clearly did not affect most tissue phase contrast (Fig. 8) Therefore we conclude that deoxyhemoglobin is not a major source of contrast neither between white and gray matter nor between the cortical layers, although some contribution cannot be ruled out. To what extent regional variations in notably higher venous blood volume fraction might affect contrast in humans through partial volume effects (not only due to the increased CBV but also to the reduced spatial resolution obtainable) remains to be determined.

The cerebral structures detected by phase imaging were readily identified on Nissl and KChIP stained slices (Fig. 7). However, on Nissl stains hippocampal contrast (apart from the dentate gyrus and other structures alike) is similar to that of white matter, which was clearly distinct in the phase images. Furthermore, the cortical layers (arrows in the phase image in Fig. 7b) are hardly visible in the Nissl stained sections. Similarly, the molecular layer and white matter of the cerebellum have similar contrast on Nissl stains but were clearly distinguishable in the phase images (Fig. 5). Therefore, the contrast mechanism underlying the phase variations is unlikely to reflect neuronal cell body density (the basis of Nissl staining).

On the other hand, KChIP staining shows little contrast between hippocampus and cortical gray matter, with both being clearly distinguishable from white matter, which is what was also observed in the phase images (Fig. 7). Likewise, the fact that cerebellar white matter, molecular and granule cell layers have different contrasts in the phase images was consistent with the distribution of voltage-gated potassium channels interacting proteins (Fig. 5f).

It was noteworthy that the frequency difference between gray and white matter in the cerebellum was significantly increased from ~3–5 Hz for the anterior commissure and surrounding white matter and most of the brain to ~15–20 Hz in the cerebellar granule layer. While this may represent marked differences in bulk susceptibility between the different structures, part of this difference may also be due to the different topology of the anterior commissure and granule cerebellar cortex. Granule cells are also known to be present in layer 4 of the cortex and regions of the hippocampus such as the dentate gyrus, all of which were clearly visible on the phase images (Fig. 7) and it remains to be determined to what extent phase image contrast reflects granule cell density.

Voltage-gated potassium channels interacting proteins are generally highly enriched in the cerebellum (Serôdio and Rudy, 1998; Strassle et al., 2005), which further supports a potential mechanistic link with KChIP. Potassium interacting proteins are a family of neuronal calcium sensor proteins (Burgoyne, 2007), and are in Ca^{2+}-free state under resting conditions. All have a high affinity for Ca^{2+}, which allows them to bind Ca^{2+} following small increases in concentration above resting levels.

Although diamagnetic calcium may at least in part contribute to the susceptibility variations, along with some contribution of macromolecular exchange mechanisms, it is more likely that the apparent correlation of the phase contrast with synaptic density (implied from the KChIP distribution) reflects an underlying correlation with tissue iron content, assuming that synaptic density is paralleled by mitochondrial density and associated heme proteins, such as cytochrome oxidase. Provided that such a link can be established, phase imaging may in addition to alterations in synaptic density provide a unique contrast reflecting tissue iron content, which has been shown to be altered in neurodegeneration by processes such as oxidative stress.

We conclude that phase imaging at high magnetic fields such as 14 T provides a unique contrast for imaging of rodent brain anatomy at a microscopic resolution in vivo. Such capabilities open the perspectives to study myelination defects, synaptic density or alterations in iron content in neurodegeneration, likely to aid in our understanding of the pathogenesis of many brain diseases.

Acknowledgments

This work was supported by Centre d'Imagerie BioMédicale (CIBM) of the UNIL, UNIGE, HUG, CHUV, EPFL and the Leenaards and Louis-Jeantet Foundations. The authors would also like to thank the help Cristina Cudalbu for her support with the scanning, Hanne Frenkel, Agathe Python and Stéphane Germain for their support with animal handling. Finally we would also like to acknowledge Arthur Magill and Wietske van der Zwaag for editorial assistance.

References

Abduljalil, A.M., Schmalbrock, P., Novak, V., Chakeres, D.W., 2003. Enhanced gray and white matter contrast of phase susceptibility-weighted images in ultra-high-field magnetic resonance imaging. J. Magn. Reson. Imaging 18, 284–290.

Aoki, I., Wu, Y.J.L., Silva, A.C., Lynch, R.M., Koretsky, A.P., 2004. In vivo detection of neuroarchitecture in the rodent brain using manganese-enhanced MRI. Neuroimage 22, 1046–1059.

Badea, A., Ali-Sharief, A.A., Johnson, G.A., 2007. Morphometric analysis of the C57BL/6J mouse brain. Neuroimage 37, 683–693.

Benveniste, H., Blackband, S.J., 2006. Translational neuroscience and magnetic-resonance microscopy. Lancet Neurol. 5, 536–544.

Benveniste, H., Kim, K., Zhang, L., Johnson, G.A., 2000. Magnetic resonance microscopy of the C57BL mouse brain. Neuroimage 11, 601–611.

Burgoyne, R.D., 2007. Neuronal calcium sensor proteins: generating diversity in neuronal Ca 2+ signalling. Nat. Rev. Neurosci. 8, 182–193.

Duyn, J.H., Van Gelderen, P., Li, T.Q., De Zwart, J.A., Koretsky, A.P., Fukunaga, M., 2007. High-field MRI of brain cortical substructure based on signal phase. Proc. Natl. Acad. Sci. U. S. A. 104, 11796–11801.

Gruetter, R., 1993. Automatic, localized in vivo adjustment of all first- and second-order shim coils. Magn. Reson. Med. 29, 804–811.
Haacke, E.M., Xu, Y., Cheng, Y.C.N., Reichenbach, J.R., 2004. Susceptibility weighted imaging (SWI). Magn. Reson. Med. 52, 612–618.
Hammond, K.E., Lupo, J.M., Xu, D., Metcalf, M., Kelley, D.A.C., Pelletier, D., Chang, S.M., Mukherjee, P., Vigneron, D.B., Nelson, S.J., 2008. Development of a robust method for generating 7.0 T multichannel phase images of the brain with application to normal volunteers and patients with neurological diseases. Neuroimage 39, 1682–1692.
Jack Jr., C.R., Garwood, M., Wengenack, T.M., Borowski, B., Curran, G.L., Lin, J., Adriany, G., Grohn, O.H., Grimm, R., Poduslo, J.F., 2004. In vivo visualization of Alzheimer's amyloid plaques by magnetic resonance imaging in transgenic mice without a contrast agent. Magn. Reson. Med. 52, 1263–1271.
Jack Jr., C.R., Wengenack, T.M., Reyes, D.A., Garwood, M., Curran, G.L., Borowski, B.J., Lin, J., Preboske, G.M., Holasek, S.S., Adriany, G., Poduslo, J.F., 2005. In vivo magnetic resonance microimaging of individual amyloid plaques in Alzheimer's transgenic mice. J. Neurosci. 25, 10041–10048.
Johnson, G.A., Ali-Sharief, A., Badea, A., Brandenburg, J., Cofer, G., Fubara, B., Gewalt, S., Hedlund, L.W., Upchurch, L., 2007. High-throughput morphologic phenotyping of the mouse brain with magnetic resonance histology. Neuroimage 37, 82–89.
Marques, J.P., Bowtell, R., 2005. Application of a Fourier-based method for rapid calculation of field inhomogeneity due to spatial variation of magnetic susceptibility. Concepts in Magnetic Resonance Part B: Magnetic Resonance Engineering 25, 65–78.
Marques, J.P., Bowtell, R.W., 2008. Using forward calculations of the magnetic field perturbation due to a realistic vascular model to explore the BOLD effect. NMR Biomed. 21, 553–565.
Mikula, S., Trotts, I., Stone, J., Jones, E.G., 2007. Internet-Enabled High-Resolution Brain Mapping and Virtual Microscopy. NeuroImage 35, 9–15.
Noll, D.C., Nishimura, D.G., Macovski, A., 1991. Homodyne detection in magnetic resonance imaging. IEEE Trans. Med. Imaging 10, 154–163.
Park, S.H., Masamoto, K., Hendrich, K., Kanno, I., Kim, S.G., 2008. Imaging brain vasculature with BOLD microscopy: MR detection limits determined by in vivo two-photon microscopy. Magn. Reson. Med. 59, 855–865.
Serôdio, P., Rudy, B., 1998. Differential expression of Kv4 K+ channel subunits mediating subthreshold transient K+ (A-type) currents in rat brain. J. Neurophysiol. 79, 1081–1091.
Shockley, R.P., LaManna, J.C., 1988. Determination of rat cerebral cortical blood volume changes by capillary mean transit time analysis during hypoxia, hypercapnia and hyperventilation. Brain Res. 454, 170–178.
Strassle, B.W., Menegola, M., Rhodes, K.J., Trimmer, J.S., 2005. Light and electron microscopic analysis of KChIP and Kv4 localization in rat cerebellar granule cells. J. Comp. Neurol. 484, 144–155.
Zhong, K., Leupold, J., von Elverfeldt, D., Speck, O., 2008. The molecular basis for gray and white matter contrast in phase imaging. Neuroimage 40, 1561–1566.